RESEARCH ON THE INFLUENCE OF DIFFERENT OBSTACLE STRUCTURES ON THE ENERGY DISTRIBUTION CHARACTERISTICS OF PULSE DETONATION GAS

by

Xiaofeng LI*, Junfeng XIAO, Feng WANG, Wei WANG, and Mengqi HU

Xi'an Thermal Power Research Institute Co., Ltd., Xi'an, China

Original scientific paper
https://doi.org/10.2298/TSCI201026194L

In order to improve the gas energy conversion efficiency at the outlet of the pulse detonation combustor, numerical calculation methods were used to study the influence of three different cross-section obstacle structures of square, circle and trapezoid on the distribution characteristics of gas pressure potential energy, kinetic energy and internal energy in a single cycle at the outlet of pulse detonation combustor. The results show that: the expansion of pulse detonation gas mainly includes three-stages: primary expansion, secondary expansion, and over-expansion. Gas pressure potential energy, kinetic energy, and internal energy increase during the primary and secondary expansion stages, and decrease during the over-expansion stage. Pulse detonation combustor with trapezoidal cross-section obstacle structure has the smallest proportion of gas energy at the outlet of the combustor during the over-expansion stage and the highest proportion during the secondary expansion stage. Compared with square and circle cross-section obstacle structures, the gas energy distribution at the outlet of the pulse detonation combustor with trapezoidal cross-section obstacle structure is the easiest for turbomachinery to convert the gas energy.

Key words: *pulse detonation combustor, detonation wave, combustion, energy, obstacle structure, expansion*

Introduction

Pulse detonation turbine engine (PDTE) is a new type of power device based on pulse detonation combustion, which is mainly composed of pulse detonation combustor (PDC), compressor and turbine. Since detonation combustion has the characteristics of self-pressurization and fast flame propagation [1], PDTE has the following advantages compared with traditional engines based on constant pressure combustion:

– high thermodynamics cycle efficiency,
– low specific fuel consumption,
– the compressor and turbine stages are few,
– the engine structure is simple, and
– the weight is reduced, and the thrust-to-weight ratio is high.

For the theoretical performance of the PDTE engine, Paxson *et al.* [2] established a 1-D numerical model to analyze the performance of the gas turbine engine after replacing the core engine with PDC. The calculation results show that if the combustion chamber is not

* Corresponding author, e-mail: wilflxf@aliyun.com

cooled, the specific fuel consumption of the engine can be reduced by 5-12 %. Andrus *et al.* [3] calculated the engine performance after replacing the main combustion chamber of a high ducted turbofan engine with PDC, and the results showed that the specific fuel consumption of the engine using PDC can be reduced by 8%. Giuliani *et al.* [4] used the CFD method to simulate the overall performance of the engine after the replacement of constant pressure combustion by detonation combustion. The results showed that the specific fuel consumption can be reduced by 5.4% after detonation combustion is used, and the engine weight can be reduced by 6 %. Lu *et al.* [5] compared and calculated the performance of engines based on detonation cycle and Brayton cycle, and pointed out that PDTE have advantages in specific thrust and fuel consumption. Li *et al.* [6, 7] used variable specific heat capacity to calculate the thermodynamics cycle efficiency of detonation cycle and Brayton cycle engine. When the temperature before the turbine is 1620 K and the pressure ratio is 16.5, the thermodynamics cycle efficiency of the PDTE engine is 28.8% higher than that of the Brayton cycle engine. In the papers [8-11] studied the matching problem of pulse detonation combustion chambers working with compressors and turbines, and the PDTE has been successfully operated for a long time in the laboratory.

The PDTE generally adopts indirect detonation method to reduce engine ignition energy, but indirect detonation method has a deflagration detonation (DDT) distance, and the structure of obstacles in the combustion chamber has a greater impact on the DDT distance. Asato *et al.* [12] studied the influence of the Shchelkin spiral obstacles on the DDT distance, and pointed out that the Shchelkin spiral obstacles can promote the generation of gas vortex, and the DDT distance can be shortened by 50-57%. Valiev *et al.* [13] stated that the physical mechanism of flame acceleration in channels with obstacles was qualitatively different from the classical Shelkin mechanism. Ogawa *et al.* [14] studied the detailed process of the transition from DDT under a square-section obstacle by numerical methods, and pointed out that the obstacle contributes to the generation of gas vortex.

The obstacle will not only affect the DDT distance, but also change the energy distribution characteristics of the outlet gas of PDC. As centripetal or axial turbines are designed based on steady-state flow conditions, and the pressure, velocity and other parameters of the gas at the outlet of PDC have strong pulsation characteristics, the turbine efficiency of PDTE is very sensitive to the energy distribution of the gas at the outlet of PDC. Therefore, studying the influence of the obstacle on the energy distribution characteristics of the pulse detonation gas at the outlet of the combustion chamber will help improve the performance of PDTE engine. In this paper, numerical calculation methods are used to study the influence of three cross-section obstacle structures of square, circle and trapezoid on the distribution characteristics of gas pressure potential energy, kinetic energy and internal energy in a single cycle at the outlet of PDC, which provides a reference for the design of turbines that convert pulse detonation gas energy.

Physical models and calculation methods

Simulation work is carried out using ANSYS FLUENT 15.0 CFD tool. Figure 1 shows a physical model of a PDC and a schematic of the three kinds of obstacles. The obstacles are installed in the detonation chamber, which can shorten the distance from DDT and enhance detonation. The inner diameter of the air inlet section of the PDC head is 100 mm, and an air intake cone and a pneumatic valve are installed inside. Fuel and atomized air are injected into the detonation chamber from the internal passage of the intake cone through the tail nozzle, and the main air enters the detonation chamber through the pneumatic valve. The detonation chamber has a diameter of 60 mm and a length of 1280 mm. The spark plug is installed in a position

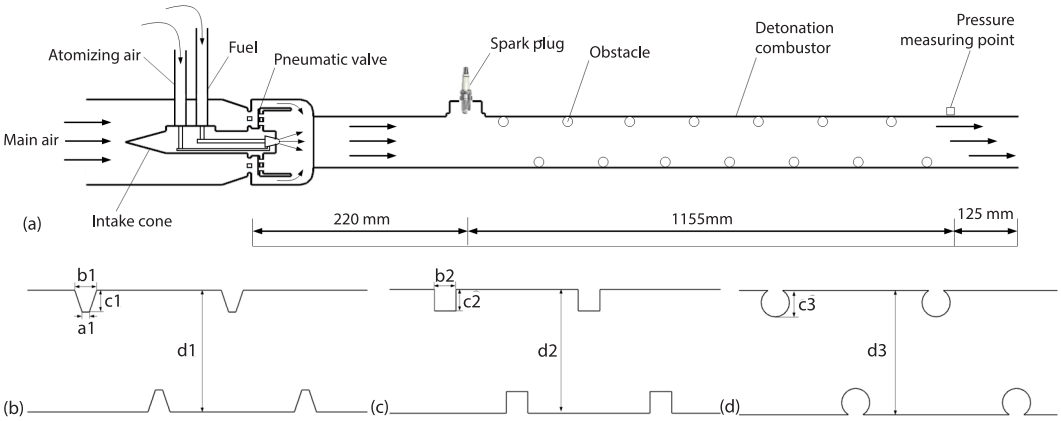

Figure 1. The PDC physical model; (a) schematic diagram of physical model of PDC, (b) trapezoidal cross-section obstacle, (c) square cross-section obstacle, and (d) circular cross-section obstacle

220 mm from the pneumatic valve, and a pressure measuring point is designed at a position 125 mm from the outlet of the detonation chamber. For trapezoidal cross-section obstacle, a_1 is 2 mm, b_1 is 6 mm, c_1 is 6 mm. For square cross-section obstacle b_2 and c_2 are both 6 mm. For circular cross-section obstacle, c_3 is 6 mm, circular cross-section diameter is 6.5 mm. For three kinds of obstacles, d_1, d_2, and d_3 are both 60 mm, and the pitch of the three kinds of obstacles is 40 mm. The test piece uses a circular cross-section obstacle structure in the detonation combustor.

According to the physical model of the PDC and the three kinds of obstacle structures, three numerical models of the PDC with different cross-sectional obstacle structures are established. The calculation domains and grid discrete methods of the three numerical models are the same. Figure 2 shows the calculation domain and grid discretization results of a PDC with a circular cross-section obstacle structure. The calculation domain includes the detonation combustor and the far field. In order to simulate the fuel and air filling process, the tail nozzle of the intake cone and pneumatic valve were modeled. The far-field with a width of 760 mm and a length of 1000 mm is set at the exit of the detonation chamber, and the axial overlap length of the far-field and the detonation chamber is 300 mm. The computational grid of the numerical model is all structured quadrilateral grid. The grid size of the detonation chamber calculation area is 1 mm, and the grid size of the far field calculation area is 3 mm. At the outlet of the detonation chamber and the pressure measuring point, there are monitoring surfaces for parameters such as pressure, temperature, speed, and so on.

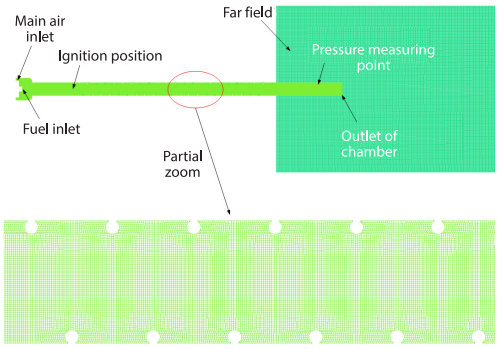

Figure 2. Computational domain and grids

The calculation methods of the three numerical models are the same. The finite volume method is used to solve the unsteady 2-D N-S equation, and the chemical reaction uses a 5-component single-step irreversible finite rate model. Considering that there is a detona-

tion enhanced obstacle structure with a large curvature change in the detonation chamber, and the realizable k-ε model has better performance than the standard k-ε model in solving strong streamline bending, vortex and rotation problems, the turbulence model uses the realizable k-ε model, and the near-wall surface is processed by the standard wall surface function. The unsteady numerical simulations are solved using the coupled algorithm. The pressure value is interpolated by PRESTO! scheme, the density value is interpolated by QUICK scheme, and the momentum and energy equations are interpolated by second-order upwind scheme. The second-order implicit scheme is selected for the time interpolation scheme.

The boundary conditions of the three numerical models are the same, which are shown in tab.1. The fuel and air inlets are both mass-flow inlet boundary conditions. The mass-flow of the main air inlet is 0.273 kg/s, and the temperature is 300 K. The mass-flow of the fuel injection port is 0.032 kg/s, the temperature is 300 K, the fuel mass-flow rate is 0.017 kg/s, the atomizing air-flow rate is 0.015 kg/s, and the fuel is n-octane. The boundary of the far field calculation area is set as the pressure outlet boundary according to the non-reflective boundary condition, the pressure value is set to 101325 Pa, and the temperature is 300 K.

Table 1. The PDC numerical model boundary conditions

Main air inlet	Fuel inlet		Far field boundary
	Atomizing air	Fuel	
0.273 kg/s 300 K	0.015 kg/s 300 K	0.017 kg/s 300 K	101325 Pa 300 K

Before starting the unsteady filling process calculations, the steady-state flow field is calculated using the given boundary conditions, and after the calculations have converged, the filling, ignition and detonation combustion unsteady processes are calculated based on the results of the steady-state flow field calculations. The unsteady calculation time step in the filling process is $1 \cdot 10^{-3}$ seconds, and the unsteady calculation time step in the ignition and detonation combustion processes is $1 \cdot 10^{-6}$ second. After the filling process is completed, a local high temperature ignition zone with a diameter of 10 mm and a temperature of 2000 K is set at the spark plug installation position.

Results and analysis

Numerical model verification

The numerical model was validated by using experimental data with the same boundary conditions as the numerical model calculation conditions. Figure 3 shows the comparison curve of the pressure numerical simulation results and the experimental measurement results at the pressure measurement points of the numerical model with a circular cross-section obstacle structure. The comparison results show that the pressure change trend obtained by the numerical simulation is the same as the test result. The numerically calculated peak detonation pressure at the pressure measurement point is 3.44 MPa, and the peak detonation pressure measured by the test is 3.12 MPa, indicating that the numerical results are consistent with the test results.

At the same time, NASA CEA software was used to verify the detonation wave velocity calculated by the numerical model. Figure 4 shows pressure curves at the pressure measurement point and the outlet of the detonation chamber. The numerical calculation results show that the time taken for the detonation wave to travel from the pressure measurement point to the detonation chamber outlet Δt is $7.899 \cdot 10^{-5}$ second. The distance between the pressure measurement point and the outlet of the detonation chamber is 125 mm, and the detonation wave

velocity is calculated to be 1582.5 m/s. The detonation wave velocity calculated by NASA CEA software is 1736.9 m/s, which is slightly higher than the numerical calculation result. This is mainly because the NASA CEA software calculates the chemical equilibrium composition and properties of the combustible mixture to obtain the Chapman-Jouguet detonation wave velocity. The calculation process does not consider the dissipation effect. Numerically, the two calculated results are close to each other, which also show that the established numerical model is reasonable.

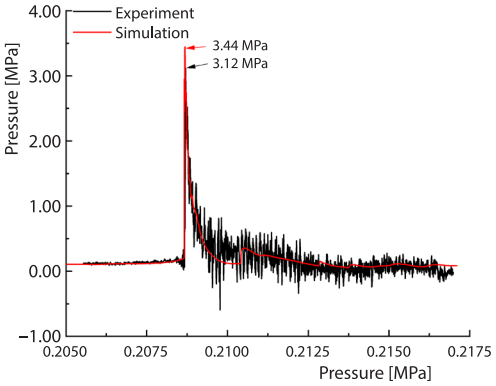

Figure 3. Comparison of pressure numerical calculation and test results at the pressure measuring point

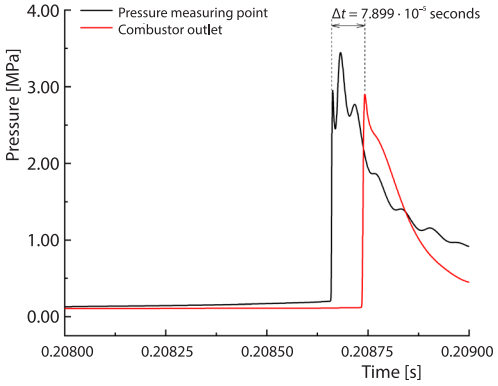

Figure 4. Pressure curves at combustor outlet and the pressure measuring point

Analysis of pulse detonation combustion gas expansion process

The expansion process of detonation gas in the detonation chamber with three different obstacle structures is similar. Figure 5 shows the pressure and velocity curves at the outlet of the PDC with square cross-section obstacles. The pressure and velocity change pattern at the outlet of the detonation chamber are analyzed. The expansion of high temperature gas formed by detonation combustion mainly includes three-stages: primary expansion, secondary expansion and over-expansion. When the detonation wave propagates to the outlet of the detonation chamber, the gas pressure and velocity at the outlet of the combustor are raised in steps. After the detonation wave passes, the pressure and velocity drop sharply, and the pressure drops more rapidly. When the compression wave reaches the outlet of the combustor, the gas pressure and velocity at the outlet of the detonation chamber increase again, and after the compression wave passes, the gas pressure and velocity at the outlet of the detonation chamber show a downward trend as a whole. When the outlet gas velocity of the combustor is lower than 0, it represents that the gas at the outlet of the combustor flows back and the gas enters the over-expansion stage. Considering that the pressure change pattern in the later stage of the primary expansion stage is similar to that of the secondary expansion stage, the definition of the secondary extension expan-

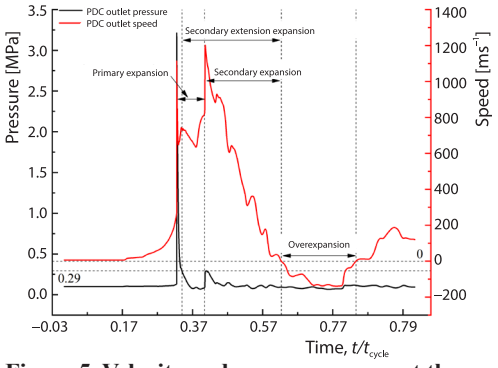

Figure 5. Velocity and pressure curves at the outlet of the PDC with square cross-section obstacles

sion stage is given in fig. 5. The point where the pressure in the primary expansion stage drops to the same value as the pressure peak in the secondary expansion stage is taken as the starting position of the secondary extension expansion stage, and the end position of the secondary expansion extension expansion stage is the same as that of the secondary expansion stage. Since the outlet gas pressure changes at this stage is smaller, the gas energy is more easily extracted and utilized by the turbine than in the primary expansion stage.

The formation of the detonation wave in the detonation chamber and the pressure change during the primary expansion stage is shown in fig. 6. The detonation wave is first formed in the tail of the detonation chamber, and then propagates to the outlet of the combustor at a shock wave velocity. Since the pressure at the head of the detonation chamber is lower than that of the detonation wave, the detonation wave propagates to the head of the detonation chamber as a compression wave while propagating to the outlet and the compression wave intensity gradually weakens during the propagation process. The back-transmitted compression wave is reflected by the head wall of the detonation chamber, forming a new compression wave that propagates to the detonation chamber outlet. When the new compression wave propagates to the exit of the combustion chamber, it enters the secondary expansion stage. The pressure change cloud diagram in the combustion chamber at this stage is shown in fig. 7. In the secondary expansion stage, the pressure at the head of the combustion chamber is greater than that at the tail of the combustion chamber. This is different from the primary expansion. In the primary expansion stage, the pressure at the head of the combustion chamber is small and the pressure at the tail of the combustion chamber is high.

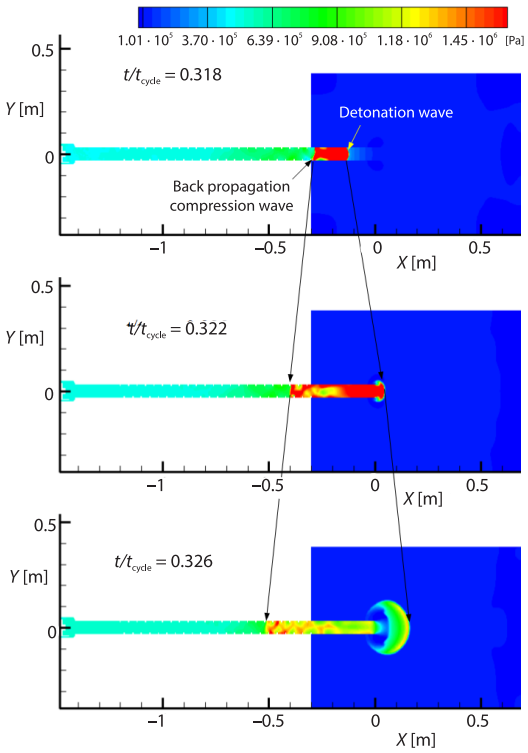

Figure 6. Pressure cloud diagram of detonation wave formation and expansion process

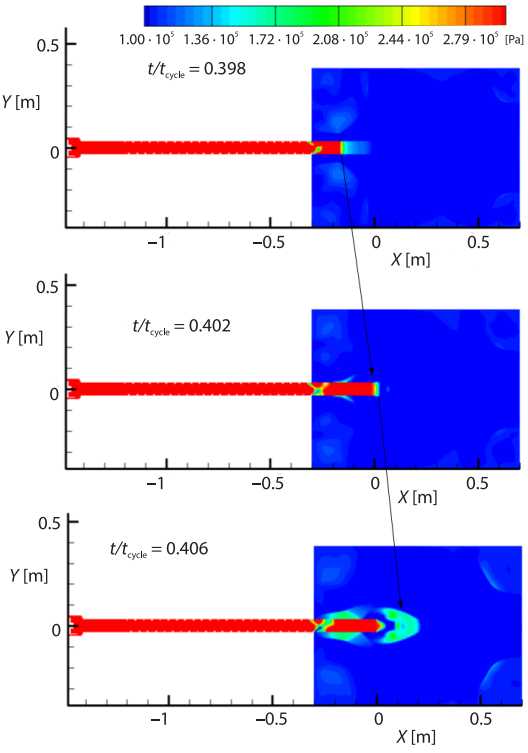

Figure 7. Pressure cloud diagram of compression wave expansion process

Analysis of the gas energy distribution at the outlet of the pulse detonation chamber

The pressure potential energy, kinetic energy, and internal energy of gas can be expressed:

$$W_p = pV$$
$$W_u = \frac{1}{2}mu_x^2 \tag{1}$$
$$W_v = c_v mT$$

where W_p, W_u, and W_v are gas pressure potential energy, kinetic energy, and internal energy, respectively, p – the gas pressure, V – the gas volume, m – the gas quality, u_x – the velocity at the outlet of detonation chamber in x-direction, c_v – the gas specific heat at constant volume, and T – the gas temperature.

In order to study the change of the gas energy at the outlet of the PDC with time, a single detonation combustion cycle is divided into multiple micro-element segments with a time interval of dt using the differential method, then the pressure potential energy, kinetic energy, and internal energy of the gas in the micro-element time period can be expressed:

$$w_p = pAu_x \mathrm{d}t$$
$$w_u = \frac{1}{2}\rho Au_x \mathrm{d}tu_x^2 = \frac{1}{2}\rho Au_x^3 \mathrm{d}t \tag{2}$$
$$w_v = c_v T \rho Au_x \mathrm{d}t$$

where A is the outlet area of the detonation chamber, ρ – the gas density, and t – the time.

Considering that the selection of dt time interval will affect the absolute value of gas energy, $w_p/\mathrm{d}t$, $w_u/\mathrm{d}t$ and $w_v/\mathrm{d}t$ are used to represent gas pressure potential energy, kinetic energy, and internal energy, respectively when studying the energy distribution.

The gas pressure potential energy, kinetic energy, and internal energy calculated by the three numerical models have the same change pattern. Figure 8 shows the curves of the gas pressure potential energy $w_p/\mathrm{d}t$ and the pressure potential energy accumulation $\int_0^t w_p$ at the outlet of the pulse detonation chamber with a square cross-section obstacle. Figure 9 presents the curves of the gas kinetic energy $w_u/\mathrm{d}t$ and the kinetic energy accumulation $\int_0^t w_u$, and fig. 10 gives the curves of the gas internal energy $w_v/\mathrm{d}t$ and the internal energy accumulation $\int_0^t w_v$. Comparing

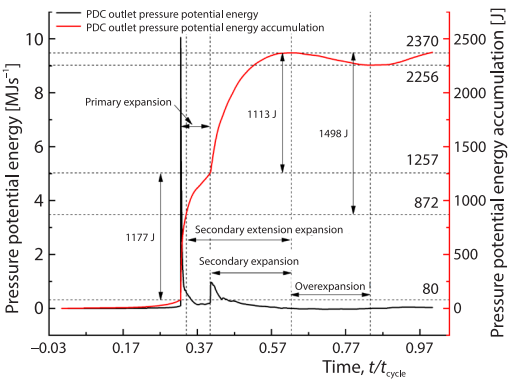

Figure 8. Pressure potential energy curves of gas at detonation chamber outlet

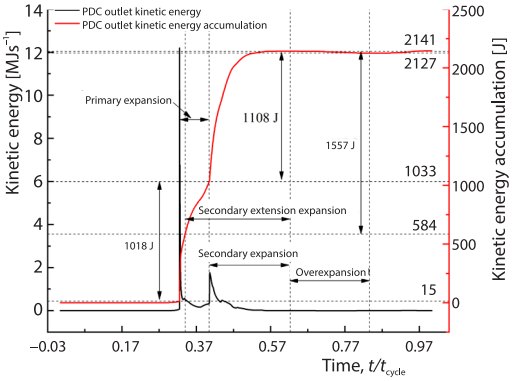

Figure 9. Kinetic energy curves of gas at detonation chamber outlet

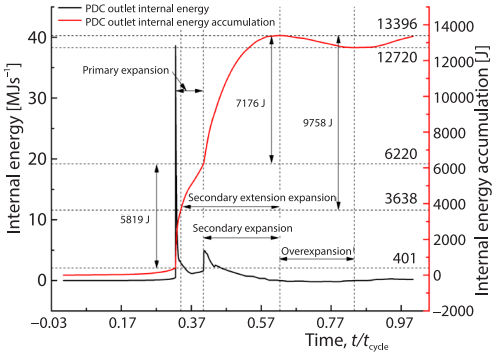

Figure 10. Internal energy curves of gas at detonation chamber outlet

the curves change trend of pressure and velocity at the outlet of the detonation chamber in fig. 5 with the pressure potential energy, kinetic energy, and internal energy in figs. 8-10, it is found that the gas pressure potential energy, kinetic energy, and internal energy change trend are consistent with the gas pressure, that is, the distribution of gas energy is mainly affected by the gas pressure. The gas pressure potential energy, kinetic energy, and internal energy accumulation curves have the same change rule, which increases in the primary and secondary expansion stages, and decreases in the over-expansion stage.

Analyzing the accumulation curve of pressure potential energy in fig. 8, it is found that the pressure potential energy in the primary and secondary expansion stages increases by 1177 J and 1113 J, respectively, accounting for 49.57% and 46.89% of the pressure potential energy in a single cycle. The pressure potential energy in the over-expansion stage decreases by 114 J, which accounts for about 4.82% of the pressure potential energy in a single cycle. The pressure potential energy in the secondary extension expansion stage increases by 1498 J and accounts for about 63.11% of the pressure potential in a single cycle.

Analyzing the accumulation curve of the gas kinetic energy in fig. 9, it is found that the kinetic energy in the primary and secondary expansion stage increases by 1018 J and 1108 J, respectively, accounting for 47.44% and 51.66% of the kinetic energy in a single cycle. The kinetic energy in the over-expansion stage decreases by 14 J, accounting for about 0.66% of the kinetic energy in a single cycle. The kinetic energy in the secondary extension expansion stage increases by 1557 J, accounting for about 72.58% of the kinetic energy in a single cycle.

Analyzing the accumulation curve of the gas internal energy in fig. 10, the internal energy in the primary and secondary expansion stage increases by 5819 J, 7176 J, respectively, accounting for about 43.59% and 53.75% of the internal energy in a single cycle, the internal energy in the over-expansion stage decreases by 676 J, accounting for about 5.06% of the internal energy in a single cycle, the internal energy in the secondary extension expansion stage of increases by 9758 J, accounting for 73.09% of the internal energy in a single cycle.

The influence of obstacle structure on the gas energy distribution at the outlet of pulse detonation chamber

The ratios of the gas pressure potential energy, kinetic energy, internal energy, and total energy at the outlet of the PDC with different cross-sectional obstacle structures in different expansion stages are shown in figs. 11-14, respectively. It is found that the energy of the exit gas of the pulse detonation chamber with trapezoidal cross-section obstacle structure accounts for the smallest proportion in the primary expansion and over-expansion stages, and the highest proportion in the secondary expansion and secondary extension expansion stages. Compared with square and circular cross-section obstacle structures, the gas energy distribution at the outlet of the PDC with trapezoidal cross-section obstacle structure is the easiest for turbomachinery to convert the gas energy.

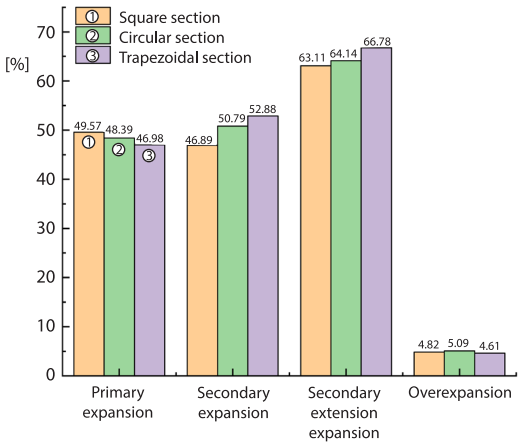

Figure 11. Pressure potential energy

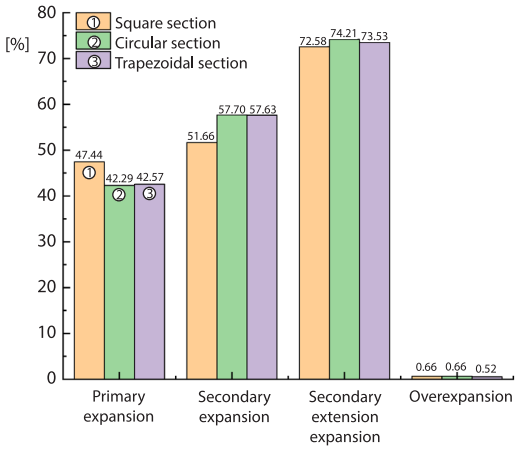

Figure 12. Kinetic energy

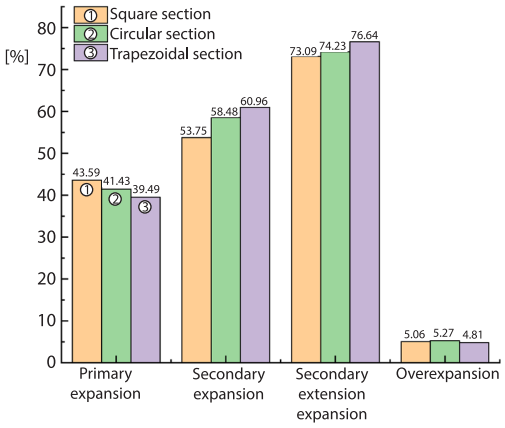

Figure 13 Internal energy

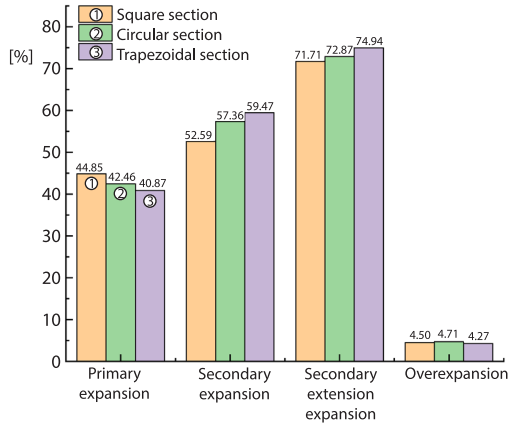

Figure 14. Total energy

Conclusions

In this paper, three numerical models of PDC with different cross-sectional shape obstacle structures are established. The distribution characteristics of the gas energy at the outlet of the PDC in a single cycle are studied, and the influence of the obstacle structure of different cross-sectional shapes on the gas energy distribution is analyzed. The following conclusions are as folows.

- The gas pressure potential energy, kinetic energy, and internal energy at the outlet of the three pulse detonation chambers with different cross-sectional shapes and obstacle structures have the same change pattern. The distribution of gas pressure potential energy, kinetic energy, and internal energy is mainly affected by the gas pressure. The gas pressure potential energy, kinetic energy, and internal energy at the outlet of the combustor all increase stepwise when the detonation wave is transmitted, and then decrease rapidly, when the compression wave expands, they suddenly rise again, and then gradually decrease.
- The expansion of pulse detonation gas mainly includes three main stages: primary expansion, secondary expansion, and over-expansion. The gas pressure potential energy, kinetic

energy and internal energy increase in the primary and secondary expansion stages, and decrease in the over-expansion stage.

- The energy of the exit gas of the PDC with trapezoidal cross-section obstacle structure accounts for the smallest proportion in the primary expansion and over-expansion stages and the highest proportion in the secondary expansion and secondary extension expansion stages. Compared with square and circular cross-section obstacle structures, the energy distribution at the outlet of the PDC with trapezoidal cross-section obstacle structure is the easiest for turbomachinery to convert the gas energy.
- In the secondary extension expansion stage, the pressure potential energy, kinetic energy, and internal energy of the gas at the outlet of the PDC with trapezoidal cross-section obstacles account for 66.78%, 73.53%, and 76.64% of the single cycle energy, respectively.

Acknowledgment

This work was financially supported by the Natural Science Foundation of Shaanxi Province of China through Grant No. 2020JQ-996.

Nomenclature

A – detonation chamber outlet area, [m^2]
c_v – gas specific heat at constant volume
m – gas quality, [kg]
p – gas pressure, [Pa]
t – time, [s]
T – gas temperature, [K]
u_x – gas velocity in x-direction, [ms^{-1}]
V – gas volume, [m^3]
W_p – gas pressure potential energy, [J]
W_u – kinetic energy, [J]
W_v – internal energy, [J]

Greek symbol

ρ – gas density, [kgm^{-3}]

Acronums

CEA – chemical equilibrium with application
DDT – deflagration detonation transition
PDC – pulse detonation combustor
PDTE – pulse detonation turbine engine

References

[1] Yan C., *et al.*, *Principle and Key Technology of Pulse Detonation Engine*, Northwestern Polytechnical University Press, Xi'an, China, 2005
[2] Paxson D. E., *et al*., Thermal Load Considerations for Detonative Combustion-Based Gas Turbine Engines, *Proceedings*, 40th AIAA/ASME/SAE/ASEE Joint Propulsion Conference and Exhibit, Fort Lauderdale, Fla., USA, 2004, AIAA 2004-3396
[3] Andrus, I. Q., *et a*l., Evaluation of a High Bypass Turbofan Hybrid Utilizing a Pulsed Detonation Combustor, *Proceedings*, 43rd AIAA/ASME/SAE/ASEE Joint Propulsion Conference and Exhibit, Cincinnati, Oh., USA, 2007, AIAA 2007-5074
[4] Giuliani, F., *et al*., Pulse Detonation as an Option for Future Innovative Gas Turbine Combustion Technologies a Concept Assessment, *Proceedings*, 27th International Congress of The Aeronautical Sciences, Nice, France, 2010, ICAS2010
[5] Lu J., *et al*., Performance Investigation of a Pulse Detonation Turbine Engine, Proceedings of the Institution of Mechanical Engineers – Part G: *Journal of Aerospace Engineering*, *230* (2016), 2, pp. 350-359
[6] Li, X., *et al.*, Thermodynamic Cycle Performance of Detonation Gas Turbine with Variable Specific Heat Capacity, *Journal of Aerospace Powe*r, *31* (2016), 2, pp. 369-376
[7] Li, X., *et al*., Ideal Thermodynamic Cycle Analysis of Gas Turbine Based on Detonation Combustion, *Journal of Northwestern Polytechnical University*, *34* (2016), 1, pp. 112-117
[8] Li, X., *et al*., Principle Experiments on Two-Phase Pulse Detonation Turbine Engine, *Journal of Aerospace Power*, *28* (2013), 12, pp. 2731-2736
[9] Qiu, H., *et al*., Tests of Pulse Detonation Turbine Engine Performance with Thrust Augmentation Devices, *Acta Aeronautica et Astronautica Sinica*, *37* (2016), 2, pp. 522-532
[10] Deng, P., *et al*., Numerical Study on Matching Mechanism and Efficiency of Pulse Detonation Combustor and Impulse Turbine, *Journal of Aerospace Power*, *38* (2018), 8, pp. 1864-1871

[11] Wang, L., *et al*., Cooperating Work Characteristics of Pulse Detonation Turbine Engine, *Journal of Aerospace Power*, *34* (2019), 3, pp. 548-555
[12] Asato, K., *et al*., Combined Effects of Vortex Flow and the Shchelkin Spiral Dimensions on Characteristics of Deflagration-to-Detonation Transition, *ShockWaves*, *23* (2013), 4, pp. 325-335
[13] Valiev, D., et al., Flame Acceleration in Channels with Obstacles in the Deflagration-to-Detonation Transition, *Combustion and Flame*, *157* (2010), 5, pp. 1012-1021
[14] Ogawa T., *et al*., Flame Acceleration and Transition Detonation in an Array of Square Obstacles, *Journal of Loss Prevention in the Process Industries*, *26* (2013), 2, pp. 355-362

Paper submitted: October 26, 2020
Paper revised: November 25, 2020
Paper accepted: February 20, 2021